RAPID COMMUNICATION | APRIL 09 2024

Finding the differences: Classical nucleation perspective on homogeneous melting and freezing of hard spheres

Willem Gispen ; Marjolein Dijkstra

J. Chem. Phys. 160, 141102 (2024)
https://doi.org/10.1063/5.0201629

The Journal of Chemical Physics COMMUNICATION pubs.aip.org/aip/jcp

Finding the differences: Classical nucleation perspective on homogeneous melting and freezing of hard spheres

Cite as: J. Chem. Phys. 160, 141102 (2024); doi: 10.1063/5.0201629
Submitted: 31 January 2024 • Accepted: 22 March 2024 •
Published Online: 9 April 2024

Willem Gispen[a] and Marjolein Dijkstra[b]

AFFILIATIONS

Soft Condensed Matter & Biophysics, Debye Institute for Nanomaterials Science, Utrecht University, Princetonplein 1, 3584 CC Utrecht, The Netherlands

[a]Author to whom correspondence should be addressed: w.h.gispen2@uu.nl
[b]E-mail: m.dijkstra@uu.nl

ABSTRACT

By employing brute-force molecular dynamics, umbrella sampling, and seeding simulations, we investigate homogeneous nucleation during melting and freezing of hard spheres. We provide insights into these opposing phase transitions from the standpoint of classical nucleation theory. We observe that melting has both a lower driving force and a lower interfacial tension than freezing. The lower driving force arises from the vicinity of a spinodal instability in the solid and from a strain energy. The lower interfacial tension implies that the Tolman lengths associated with melting and freezing have opposite signs, a phenomenon that we interpret with Turnbull's rule. Despite these asymmetries, the nucleation rates for freezing and melting are found to be comparable.

Melting and freezing are opposing pathways by which matter transitions between solid and liquid phases. These processes have significant implications across various scientific disciplines, including materials science, geophysics, biology, and atmospheric sciences. Understanding them is crucial in numerous practical applications. For instance, in metallurgy, knowledge of freezing and melting is essential for processes such as casting, welding, and shaping. In the pharmaceutical industry, crystallization and melting play a crucial role in influencing the solubility and formulation of drugs.

Both melting and freezing most commonly occur through heterogeneous nucleation on external surfaces or internal defects. Nonetheless, homogeneous nucleation remains a useful starting point for understanding the thermodynamics of these first-order phase transitions. For example, knowledge of the homogeneous freezing rate can be used to predict the heterogeneous freezing rate.[1] Experimentally, the involvement of surfaces and defects makes the study of homogeneous melting and freezing challenging. However, it is possible to mitigate these effects, for instance, external surfaces can be coated,[2] and defects can be annealed using heating cycles.[3] This has enabled the experimental observation of homogeneous melting in a system of thermally responsive microgel colloids.[3–5]

The key factor in homogeneous nucleation is the nucleation rate. Classical nucleation theory (CNT) plays a paramount role for qualitatively understanding this rate. CNT consists of three components, the driving force, interfacial tension, and kinetic prefactor. Notably, the kinetic prefactor and driving force can be accurately determined using the bulk equations of state. This leaves the interfacial tension as the primary unknown in CNT. Phenomenological rules exist for predicting trends in the interfacial tension. For instance, Turnbull's phenomenological rule[6] asserts that the interfacial tension is proportional to the melting enthalpy. Additionally, Tolman[7] argued that it varies with the curvature of the interface.

In the past two decades, it has become possible to test these predictions using computer simulations. These simulations provide a unique tool for uncovering the mechanisms and thermodynamics of nucleation. For instance, Sanchez-Burgos *et al.*[8] demonstrated that the Tolman length is equivalent for condensation and cavitation. However, much less is known about the interfacial tension governing the melting transition and whether a similar symmetry exists between freezing and melting. One reason for this knowledge gap is that melting has traditionally been considered a one-sided instability of the solid phase, with most research focusing on the

role of various types of defects that lead to catastrophic melting at the limit of superheating.[9–14] Due to the emphasis on the superheat limit, numerous unresolved questions persist regarding the mechanism and thermodynamics of melting prior to reaching the superheat limit. Furthermore, the focus on defects has cast significant doubts on the suitability of CNT for effectively describing the melting process.[9,10,14] For example, it has never been tested whether CNT can successfully predict the melting rate.

In this Communication, we assess the applicability of CNT in describing melting and freezing of hard spheres. Using computer simulations, we investigate homogeneous melting and freezing within the solid–fluid coexistence region. Our findings reveal several asymmetries between melting and freezing, offering a unique perspective on the predictions of Turnbull and Tolman.

We first perform molecular dynamics simulations to elucidate the mechanism of homogeneous melting. We prepare a surface-free and defect-free face-centered cubic (fcc) crystal consisting of $N = 2 \times 10^4$ nearly hard spheres that interact with a Weeks–Chandler–Andersen (WCA) potential. This potential has been extensively used in previous research for modeling hard spheres via molecular dynamics. Specifically, prior studies[15,16] have shown that this potential effectively maps freezing rates to hard spheres when defining an effective hard-sphere diameter σ_{eff} such that the freezing density[15] aligns with that of hard spheres.[17]

In the following, we use this effective hard-sphere diameter to calculate the effective packing fraction $\eta = N\pi\sigma_{\text{eff}}^3/6\ V$. We perform all our simulations in the coexistence region between the freezing point $\eta_{\text{fr}} = 0.492$ and melting point $\eta_{\text{m}} = 0.544$.[17] First, we perform brute-force canonical ensemble (NVT) simulations of the fcc crystal from $\eta = 0.503$–0.508. In Fig. 1, we show a fluid nucleus at $\eta = 0.508$. For comparison, we also show a crystal nucleus from previous simulations[16] at $\eta = 0.528$. We differentiate between fluid-like (dark blue) and solid-like (yellow) particles using the averaged Steinhardt bond order parameter $\bar{q}_6$.[18] Employing the mislabeling scheme,[19] we calculate a pressure-dependent threshold $\bar{q}_6^*(P)$ and classify particles as fluid-like when $\bar{q}_6 < \bar{q}_6^*(P)$ and solid-like when $\bar{q}_6 > \bar{q}_6^*(P)$. For additional details, refer to the supplementary material. Similar to freezing, the fluid nucleus depicted in Fig. 1 has an approximately spherical shape. We did not observe nuclei with a lentil or oblate shape, not even in the region close to the melting point where they are theoretically predicted.[25,26] See the supplementary material for additional illustrations of the shapes of the fluid nuclei. Therefore, we assume a spherical shape in our subsequent analysis. The formation of a nucleus can take a long time, but once it reaches a critical size, it rapidly expands, leading to melting of the entire system. This observation that melting follows a nucleation and growth scenario aligns with prior findings[9] and reinforces the applicability of CNT.

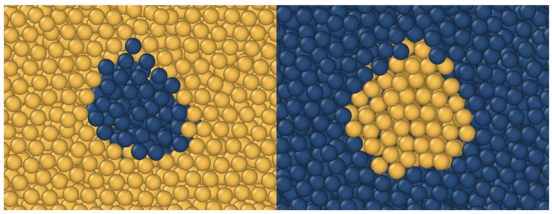

FIG. 1. Cut-through images of nucleation during homogeneous melting (left) and freezing (right) of hard spheres. The nuclei are identified using the Steinhardt bond order parameter $\bar{q}_6$. Yellow corresponds to solid-like particles, and dark blue corresponds to fluid-like particles.

To quantitatively describe the thermodynamics of melting and freezing using CNT, we first calculate the driving force for nucleation, which is determined by the difference in chemical potential $|\Delta\mu|$ between the fluid and solid phase. We calculate this difference by employing thermodynamic integration of empirical equations of state[9,27] from coexistence.[17] In Fig. 2, we present the driving force $|\Delta\mu|$ for both the melting and freezing of hard spheres as a function of packing fraction η. Surprisingly, the driving force for melting is significantly lower than that for freezing. According to the Gibbs–Duhem equation $\partial|\Delta\mu|/\partial P = \Delta(1/\rho)$, the derivative $\partial|\Delta\mu|/\partial P$ should be nearly equal for melting and freezing. However, within the solid–fluid coexistence region, the pressure of the solid changes much less than that of the fluid. To illustrate this, we also plot the pressure difference from coexistence $\beta|P - P_{\text{coex}}|\sigma^3$ in Fig. 2. The reduced pressure variation for the solid phase is associated with the spinodal instability occurring at $\eta = 0.494$,[9] where, by definition, the derivative $\partial P/\partial\eta$ becomes zero. In summary, the primary reason for the lower driving force for melting is the presence of a spinodal instability. However, the driving force for melting is also reduced by strain energy.[28–31] The reduced density within a fluid nucleus compels the surrounding crystal to deform, incurring an additional free-energy cost that is proportional to the volume of the fluid nucleus,

$$\Delta G = \gamma 4\pi r^2 - |\Delta\mu|\frac{4\pi}{3}r^3\rho_f + E_{\text{strain}}\frac{4\pi}{3}r^3. \tag{1}$$

Here, ΔG denotes the Gibbs free energy for nucleation, γ is the solid–fluid interfacial tension, and r and ρ_f are the radius and density of the fluid nucleus, respectively. Additionally, E_{strain} corresponds to the strain energy given by

$$E_{\text{strain}} = \frac{2C_s B_f}{4C_s + 3B_f}\left(\frac{1/\eta_f - 1/\eta_s}{1/\eta_s}\right)^2. \tag{2}$$

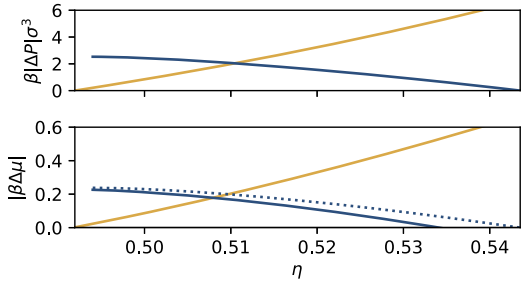

FIG. 2. Top: Pressure difference from coexistence $\beta|P - P_{\text{coex}}|\sigma^3$ for the fluid (yellow) and solid (dark blue) phase of hard spheres as a function of packing fraction η. Bottom: Driving force for melting and freezing as a function of packing fraction η. The yellow line is the difference in chemical potential between the solid and fluid phase as a function of the packing fraction of the fluid phase. The blue dotted line is the chemical potential difference as a function of the packing fraction of the solid phase. The blue solid line is the effective driving force $|\Delta\mu_{\text{eff}}| = |\Delta\mu| - E_{\text{strain}}/\rho_f$ for melting.

In this expression, C_s represents the shear modulus of the solid,[9] B_f represents the bulk modulus of the fluid,[27] and the term within brackets denotes the relative volume change due to melting. This expression for the strain energy is based on a calculation using the continuum theory of elasticity.[28] The strain energy lowers the effective driving force $|\Delta\mu_{\text{eff}}| = |\Delta\mu| - E_{\text{strain}}/\rho_f$. Given the very low driving force for melting, it is surprising that we have observed spontaneous melting at $\eta_{\text{eff}} = 0.508$, where the effective driving force is $0.18k_BT$. In contrast, spontaneous freezing can only be observed at $\eta \geq 0.528$,[16] where the driving force is $\geq 0.44\ k_BT$.

To understand this surprising asymmetry, we separate thermodynamics from kinetics. Starting from a perfect fcc lattice, we measure the Gibbs free-energy barrier $\beta\Delta G(n)$ required to form a fluid nucleus of size n using the umbrella sampling technique.[32] In Fig. 3, we present these free-energy barriers for three different pressures, corresponding to effective driving forces $|\beta\Delta\mu_{\text{eff}}| = 0.14, 0.15$, and 0.18. According to CNT, the barrier height ΔG^* and critical nucleus size n^* are related as $\Delta G^* = n^*|\Delta\mu_{\text{eff}}|/2$. We plot this CNT approximation as blue dots in Fig. 3, showing that it is a reasonable approximation for the height of the barrier, with a maximum error of $5k_BT$ at the lowest supersaturation. We note that CNT can be adjusted to describe the shape and height of the nucleation barrier more accurately.[33–36] In Fig. 3, we also display the freezing barriers computed by Auer and Frenkel.[32] When we compare their freezing barriers with our melting barriers, we observe that the critical nucleus size for melting is much larger than for freezing. For instance, the freezing barrier at $|\beta\Delta\mu| = 0.34$ and the melting barrier at $|\beta\Delta\mu_{\text{eff}}| = 0.15$ both have a height of $\sim 42k_BT$, but the critical nucleus size is ~590 for melting and 230 for freezing. The same comparison reveals that melting has a significantly lower effective driving force for a nucleation barrier of comparable height.

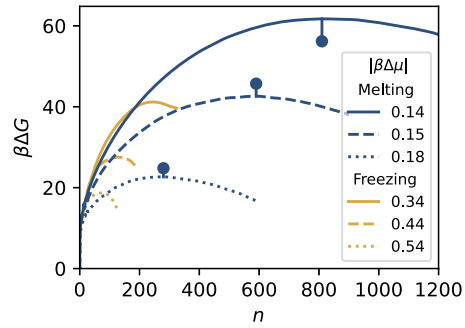

FIG. 3. Gibbs free energy $\beta\Delta G$ as a function of nucleus size n for melting and freezing as obtained from umbrella sampling for three different driving forces $\beta\Delta\mu$. The freezing barriers (yellow) are taken from the work of Auer and Frenkel.[32] The melting barriers (blue) are determined in this work. For melting, the blue dots are the CNT approximations of the barrier height $\Delta G^* = n^*|\Delta\mu_{\text{eff}}|/2$, with n^* being the critical nucleus size.

From a CNT perspective, this implies that the interfacial tension for melting must be lower than for freezing. We calculate the interfacial tension using CNT based on brute-force,[16] seeding,[19] and umbrella sampling[34] simulations; see the supplementary material. In Fig. 4(a), we plot the interfacial tension γ as a function of the inverse critical radius $1/r^*$ for both freezing and melting.

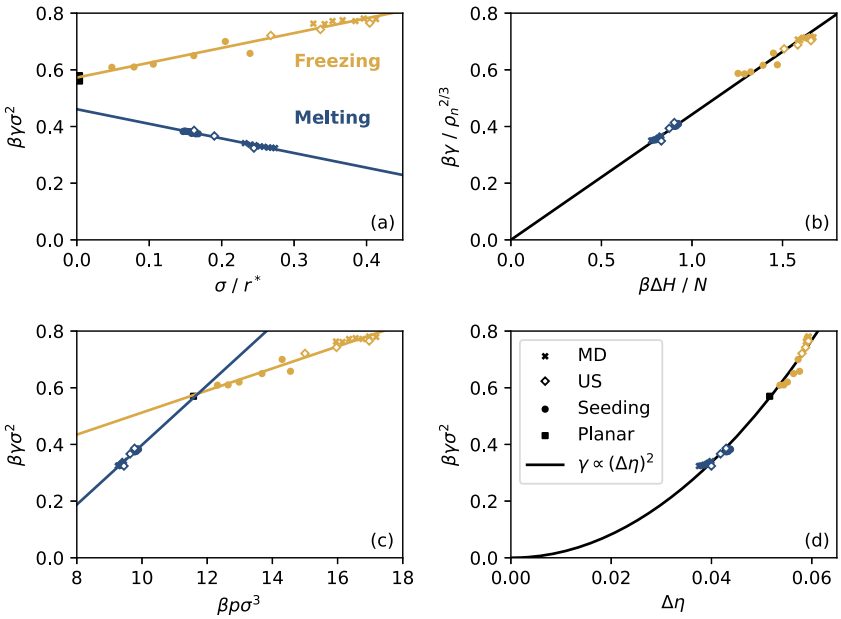

FIG. 4. Interfacial tension γ as a function of (a) inverse critical radius σ/r^*, (b) enthalpy difference $\beta\Delta H/N$ between fluid and solid, (c) pressure $\beta p\sigma^3$, and (d) difference in packing fraction η between fluid and solid. The interfacial tension is calculated using CNT from molecular dynamics (MD, crosses), umbrella sampling (US, diamonds), and seeding (circles). The lines are either linear (a), (b), and (c) or power law (d) fits of the data. For freezing, we used data from the works of Gispen and Dijkstra[16] (MD), Espinosa *et al.*[19] (seeding), and Filion *et al.*[34] (US). Following Turnbull,[6] we normalize γ with the density ρ_n of the nucleating phase for (b).

We see that the interfacial tension for freezing converges to the planar limit $\beta\gamma\sigma^2 = 0.57$[37] as $1/r^* \to 0$, whereas it extrapolates to a lower value for melting, which may be associated with the strain energy. Clearly, the common assumption of a constant interfacial tension[9,30,38,39] is not suitable for hard spheres since the interfacial tension increases with $1/r^*$ for freezing,[40,41] whereas it decreases for melting. Our results for the interfacial tension for melting deviate from the experimental value of $\beta\gamma\sigma^2 = 0.84$ estimated from homogeneous nucleation,[5] but align well with the experimental value of $\beta\gamma\sigma^2 = 0.42$ estimated from nucleus growth.[3] Qualitatively, our observation of a decreasing interfacial tension for melting is consistent with previous simulations of a Lennard-Jones system.[31,42] Based on linear fits of the interfacial tension, we can estimate the Tolman lengths as -0.46σ for freezing and 0.56σ for melting. Interestingly, we observe that the Tolman length has opposite signs but similar magnitudes for freezing and melting. In the context of boiling and condensation, opposite signs of the Tolman length have been attributed to the transition from a convex to a concave surface, i.e., a shift from positive to negative curvature.[43]

To understand the origin of this asymmetry in the interfacial tension, we invoke Turnbull's phenomenological rule,[6] which states that the interfacial tension is proportional to the difference in enthalpy between the solid and fluid phases. In Fig. 4(b), we show the interfacial tension γ as a function of this enthalpy difference ΔH. Following Turnbull, we normalize γ with the density ρ_n of the nucleating phase to the power 2/3. We see that γ is indeed approximately proportional to ΔH. Alternatively, we can understand the lower interfacial tension by examining how it scales with the pressure $\beta p\sigma^3$ or the difference in packing fraction $\Delta\eta$ between the solid and fluid phases. In Fig. 4(c), we show the variation of interfacial tension with pressure. It is described well by two linear relations, one for melting and one for freezing, that intersect at the coexistence pressure. The increase of interfacial tension with pressure has previously been attributed to the pV work that is needed to accommodate the less efficient packing of particles near the solid–fluid interface.[44] In Fig. 4(d), we plot the dependence of interfacial tension on the difference in packing fraction. The best power-law fit of this dependence yields an exponent of 2.02, which reasonably describes the interfacial tension. The power-law scaling of the interfacial tension with the density difference is reminiscent of the scaling laws for surface tension near a gas–liquid critical point.[45] However, it is important to note that both Turnbull's rule and the scaling laws near a critical point are not specifically intended to describe the variation of fluid–solid interfacial tension with supersaturation. Nevertheless, they provide some insights into why the interfacial tension is lower for melting: the differences in density and enthalpy quantify the extent to which the density and structure of the two phases must change across the fluid–solid interface. Because these differences are much smaller for melting, it explains why the interfacial tension is also lower.

So far, we have interpreted our brute-force and umbrella sampling simulations using CNT and have shown there are significant asymmetries between freezing and melting concerning driving force and interfacial tension. However, how does this translate to the most important quantity, which is also experimentally accessible, the nucleation rate? Can CNT be employed to *predict* the nucleation rate as well? To address these questions, we use fluid nuclei that were equilibrated with umbrella sampling simulations as initial configurations for seeding simulations.[19] For eight different seeds, ranging in size from $n = 800$–1200, we determine the driving force necessary to make these seeds critical. In this way, we obtain the critical nucleus size n^* as a function of the driving force. From the critical nucleus size and the driving force, we can compute the interfacial tension. The seeding results for the interfacial tension are fitted linearly as a function of pressure, as illustrated in Fig. 4(c). In this way, we account for the influence of finite size, curvature, and pressure on the interfacial tension.[19,46] From the fit, we can then compute the nucleation barrier ΔG^* as a function of pressure. Subsequently, the CNT prediction for the nucleation rate is expressed as $J = J_0 \exp(-\Delta G^*/kT)$, where J_0 denotes the kinetic prefactor. From the seeding simulations, we determine that $J_0 \approx 50 D_L$, where D_L is the long-time diffusion coefficient of the fluid phase. This kinetic prefactor is very similar to the kinetic prefactor for freezing, and we assume it to remain constant within the fluid–solid coexistence region. Using this knowledge, we can now make CNT predictions for the nucleation rate within the full fluid–solid coexistence region; see the supplementary material for additional details.

In Fig. 5, we plot the nucleation rates for freezing and melting, as evaluated using brute-force molecular dynamics (MD), umbrella sampling (US), and seeding. The CNT predictions are shown with solid lines. For freezing, we show previously published results,[15,16,19] while the melting rates are all original. It is worth repeating that CNT has been argued to provide highly inaccurate nucleation rate predictions, with discrepancies reaching as high as ten orders of magnitude. Previous observations of the role of defects in the melting mechanism have also cast significant doubts on the suitability of CNT.[9,10,14] However, we find that the CNT prediction of the melting rate via seeding agrees very well with our brute-force and umbrella

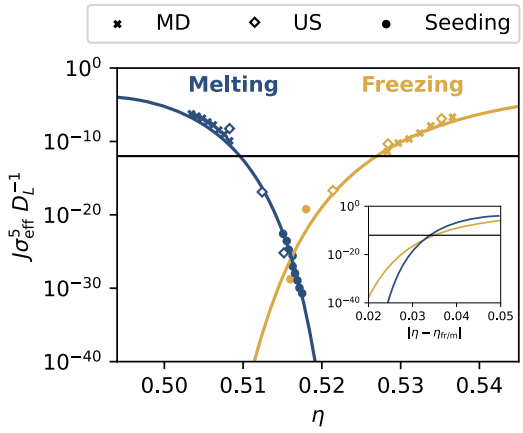

FIG. 5. Nucleation rate $J\sigma_{\rm eff}^5/D_L$ of freezing and melting as a function of packing fraction η, where D_L denotes the long-time diffusion coefficient. We show brute-force molecular dynamics (MD, crosses), umbrella sampling (US, diamonds), and seeding (circles and lines) predictions for the nucleation rate. The results for melting are from this work; the results for freezing are taken from the works of Espinosa *et al.*[19] (seeding), Filion *et al.*[34] (US), and Gispen and Dijkstra[16] (MD). The horizontal solid line is an approximate lower limit $J\sigma_{\rm eff}^5/D_L = 10^{-12}$ to what is accessible to experiments on colloidal hard spheres.[37] The inset shows the nucleation rate as a function of packing fraction difference from the freezing point $\eta_{\rm fr}$ and melting point $\eta_{\rm m}$, respectively.

sampling simulations. This good agreement was previously shown for freezing as well.[16,19]

These results indicate that when measuring the dependence of interfacial tension on curvature and pressure using seeding,[19,46] CNT can offer excellent predictions for the nucleation rate for both melting and freezing of hard spheres. In the inset of Fig. 5, we compare the nucleation rates at equal packing fraction differences from the freezing point $\eta_{fr} = 0.492$ and melting point $\eta_m = 0.544$, respectively.[17] Despite the differences in driving force and interfacial tension, the nucleation rate exhibits a fairly symmetric behavior. Particularly within the regime $|\eta - \eta_{f/m}| > 0.034$, the freezing and melting rates are very comparable, with a difference of less than two orders of magnitude. Conversely, within the regime $|\eta - \eta_{f/m}| < 0.034$, the nucleation rate $J\sigma_{eff}^5/D_L$ for both melting and freezing falls below 10^{-12}. This value serves as an approximate limit for what can be experimentally observed with colloidal hard spheres.[37] Consequently, this region $|\eta - \eta_{f/m}| < 0.034$ or equivalently $0.51 < \eta < 0.526$ represents a 'forbidden zone' for homogeneous nucleation of colloidal hard spheres. Our results suggest that when phase transitions are observed in this regime, whether it is melting or freezing, it cannot be homogeneous nucleation, but must be some form of heterogeneous nucleation.

In conclusion, we have studied homogeneous melting and freezing of hard spheres, with particular focus on the thermodynamic factors employed in classical nucleation theory. We have identified several reasons for the asymmetry between melting and freezing, such as the vicinity of a spinodal instability in the solid phase and the strain energy associated with melting. Moreover, melting exhibits both a lower driving force and a lower interfacial tension in comparison to freezing. This interfacial tension asymmetry is characterized by similar-magnitude but opposite-sign Tolman lengths for freezing and melting. We have interpreted this asymmetry through Turnbull's rule and a scaling law. Remarkably, the asymmetries in driving force and interfacial tension roughly offset each other. When comparing the nucleation rates of freezing and melting at equal packing fraction differences from the freezing and melting lines, respectively, we find that both processes exhibit roughly similar nucleation rates. It would be interesting to investigate whether the asymmetries we find between melting and freezing of hard spheres are also present in more complex systems, such as water. Our discovery that classical nucleation theory, augmented with an elastic strain energy correction, accurately predicts the homogeneous melting rate and holds promise for transferring it to the study of melting phenomena in atomic, molecular, and colloidal systems.

SUPPLEMENTARY MATERIAL

See the supplementary material for the code, details on bond orientational order parameters, molecular dynamics simulations, umbrella sampling, and seeding simulations, which includes Refs. 20–24.

ACKNOWLEDGMENTS

We thank Eduardo Sanz and Patrick Charbonneau for useful discussions and suggestions. M.D. and W.G. acknowledge funding from the European Research Council (ERC) under the European Union's Horizon 2020 Research and Innovation Program (Grant Agreement No. ERC-2019-ADG 884902 SoftML).

AUTHOR DECLARATIONS

Conflict of Interest

The authors have no conflicts to disclose.

Author Contributions

Willem Gispen: Conceptualization (equal); Data curation (equal); Formal analysis (equal); Investigation (equal); Methodology (equal); Software (equal); Visualization (equal); Writing – original draft (equal); Writing – review & editing (equal). **Marjolein Dijkstra**: Conceptualization (equal); Funding acquisition (equal); Project administration (equal); Resources (equal); Supervision (equal); Writing – review & editing (equal).

DATA AVAILABILITY

The data that support the findings of this study are available within the article and its supplementary material.

REFERENCES

[1] T. Yuan, R. S. DeFever, J. Zhou, E. C. Cortes-Morales, and S. Sarupria, "RSeeds: Rigid seeding method for studying heterogeneous crystal nucleation," J. Phys. Chem. B **127**, 4112–4125 (2023).
[2] J. Daeges, H. Gleiter, and J. H. Perepezko, "Superheating of metal crystals," Phys. Lett. A **119**, 79–82 (1986).
[3] Z. Wang, F. Wang, Y. Peng, and Y. Han, "Direct observation of liquid nucleus growth in homogeneous melting of colloidal crystals," Nat. Commun. **6**, 6942 (2015).
[4] A. M. Alsayed, M. F. Islam, J. Zhang, P. J. Collings, and A. G. Yodh, "Premelting at defects within bulk colloidal crystals," Science **309**, 1207–1210 (2005).
[5] Z. Wang, F. Wang, Y. Peng, Z. Zheng, and Y. Han, "Imaging the homogeneous nucleation during the melting of superheated colloidal crystals," Science **338**, 87–90 (2012).
[6] D. Turnbull, "Formation of crystal nuclei in liquid metals," J. Appl. Phys. **21**, 1022–1028 (1950).
[7] R. C. Tolman, "The effect of droplet size on surface tension," J. Chem. Phys. **17**, 333–337 (1949).
[8] I. Sanchez-Burgos, P. M. de Hijes, P. Rosales-Pelaez, C. Vega, and E. Sanz, "Equivalence between condensation and boiling in a Lennard-Jones fluid," Phys. Rev. E **102**, 062609 (2020).
[9] F. Wang, Z. Wang, Y. Peng, Z. Zheng, and Y. Han, "Homogeneous melting near the superheat limit of hard-sphere crystals," Soft Matter **14**, 2447–2453 (2018).
[10] S. N. Charaborty, S. Talapatra, and C. Chakravarty, "Relationship between crystalline order and melting mechanisms of solids," Indian J. Phys. **83**, 65–79 (2009).
[11] M. Forsblom and G. Grimvall, "How superheated crystals melt," Nat. Mater. **4**, 388–390 (2005).
[12] L. Gómez, A. Dobry, C. Geuting, H. T. Diep, and L. Burakovsky, "Dislocation lines as the precursor of the melting of crystalline solids observed in Monte Carlo simulations," Phys. Rev. Lett. **90**, 095701 (2003).
[13] Z. H. Jin, P. Gumbsch, K. Lu, and E. Ma, "Melting mechanisms at the limit of superheating," Phys. Rev. Lett. **87**, 055703 (2001).
[14] A. Samanta, M. E. Tuckerman, T.-Q. Yu, and W. E, "Microscopic mechanisms of equilibrium melting of a solid," Science **346**, 729–732 (2014).

[15]L. Filion, R. Ni, D. Frenkel, and M. Dijkstra, "Simulation of nucleation in almost hard-sphere colloids: The discrepancy between experiment and simulation persists," J. Chem. Phys. **134**, 134901 (2011).
[16]W. Gispen and M. Dijkstra, "Brute-force nucleation rates of hard spheres compared with rare-event methods and classical nucleation theory," J. Chem. Phys. **159**, 086101 (2023).
[17]D. Frenkel and B. Smit, *Understanding Molecular Simulation: From Algorithms to Applications* (Elsevier, 2001), Vol. 1.
[18]W. Lechner and C. Dellago, "Accurate determination of crystal structures based on averaged local bond order parameters," J. Chem. Phys. **129**, 114707 (2008).
[19]J. R. Espinosa, C. Vega, C. Valeriani, and E. Sanz, "Seeding approach to crystal nucleation," J. Chem. Phys. **144**, 034501 (2016).
[20]S. Plimpton, "Fast parallel algorithms for short-range molecular dynamics," J. Comput. Phys. **117**, 1–19 (1995).
[21]P. J. Steinhardt, D. R. Nelson, and M. Ronchetti, "Bond-orientational order in liquids and glasses," Phys. Rev. B **28**, 784–805 (1983).
[22]V. Ramasubramani, B. D. Dice, E. S. Harper, M. P. Spellings, J. A. Anderson, and S. C. Glotzer, "freud: A software suite for high throughput analysis of particle simulation data," Comput. Phys. Commun. **254**, 107275 (2020).
[23]J. A. Anderson, J. Glaser, and S. C. Glotzer, "HOOMD-blue: A Python package for high-performance molecular dynamics and hard particle Monte Carlo simulations," Comput. Mater. Sci. **173**, 109363 (2020).
[24]J. Kastner and W. Thiel, "Bridging the gap between thermodynamic integration and umbrella sampling provides a novel analysis method: 'Umbrella integration,'" J. Chem. Phys. **123**, 144104 (2005).
[25]E. A. Brener, S. V. Iordanskii, and V. I. Marchenko, "Elastic effects on the kinetics of a phase transition," Phys. Rev. Lett. **82**, 1506–1509 (1999).
[26]V. I. Motorin and S. L. Musher, "Kinetics of the volume melting. Nucleation and superheating of metals," J. Chem. Phys. **81**, 465–469 (1984).
[27]H. Liu, "Carnahan-Starling type equations of state for stable hard disk and hard sphere fluids," Mol. Phys. **119**, e1886364 (2021).
[28]J. Eshelby, *The Continuum Theory of Lattice Defects* (Academic Press, 1956), pp. 79–144.
[29]Z. Jin and K. Lu, "Melting of surface-free bulk single crystals," Philos. Mag. Lett. **78**, 29–35 (1998).
[30]K. Lu and Y. Li, "Homogeneous nucleation catastrophe as a kinetic stability limit for superheated crystal," Phys. Rev. Lett. **80**, 4474–4477 (1998).
[31]X.-M. Bai and M. Li, "Nature and extent of melting in superheated solids: Liquid-solid coexistence model," Phys. Rev. B **72**, 052108 (2005).
[32]S. Auer and D. Frenkel, "Prediction of absolute crystal-nucleation rate in hard-sphere colloids," Nature **409**, 1020–1023 (2001).
[33]J. Merikanto, E. Zapadinsky, A. Lauri, and H. Vehkamäki, "Origin of the failure of classical nucleation theory: Incorrect description of the smallest clusters," Phys. Rev. Lett. **98**, 145702 (2007).
[34]L. Filion, M. Hermes, R. Ni, and M. Dijkstra, "Crystal nucleation of hard spheres using molecular dynamics, umbrella sampling, and forward flux sampling: A comparison of simulation techniques," J. Chem. Phys. **133**, 244115 (2010).
[35]S. Prestipino, A. Laio, and E. Tosatti, "Systematic improvement of classical nucleation theory," Phys. Rev. Lett. **108**, 225701 (2012).
[36]W. Gispen, J. R. Espinosa, E. Sanz, C. Vega, and M. Dijkstra, "Variational umbrella seeding for calculating nucleation barriers," arXiv:2402.13892 (2024).
[37]C. P. Royall, P. Charbonneau, M. Dijkstra, J. Russo, F. Smallenburg, T. Speck, and C. Valeriani, "Colloidal hard spheres: Triumphs, challenges and mysteries," arXiv:2305.02452 (2023).
[38]S.-N. Luo, A. Strachan, and D. C. Swift, "Nonequilibrium melting and crystallization of a model Lennard-Jones system," J. Chem. Phys. **120**, 11640–11649 (2004).
[39]B. Rethfeld, K. Sokolowski-Tinten, D. von der Linde, and S. I. Anisimov, "Ultrafast thermal melting of laser-excited solids by homogeneous nucleation," Phys. Rev. B **65**, 092103 (2002).
[40]P. Montero de Hijes, J. R. Espinosa, E. Sanz, and C. Vega, "Interfacial free energy of a liquid-solid interface: Its change with curvature," J. Chem. Phys. **151**, 144501 (2019).
[41]P. Montero de Hijes, J. R. Espinosa, V. Bianco, E. Sanz, and C. Vega, "Interfacial free energy and Tolman length of curved liquid–solid interfaces from equilibrium studies," J. Phys. Chem. C **124**, 8795–8805 (2020).
[42]V. G. Baidakov and A. O. Tipeev, "The kinetics of the liquid phase nucleation in a stretched FCC crystal: A molecular dynamics simulation," Phys. Solid State **60**, 1853–1860 (2018).
[43]K. Binder and P. Virnau, "Overview: Understanding nucleation phenomena from simulations of lattice gas models," J. Chem. Phys. **145**, 211701 (2016).
[44]J. A. van Meel, B. Charbonneau, A. Fortini, and P. Charbonneau, "Hard-sphere crystallization gets rarer with increasing dimension," Phys. Rev. E **80**, 061110 (2009).
[45]J. S. Rowlinson and B. Widom, *Molecular Theory of Capillarity* (Clarendon Press, Oxford, 1989).
[46]T. Zykova-Timan, C. Valeriani, E. Sanz, D. Frenkel, and E. Tosatti, "Irreducible finite-size effects in the surface free energy of NaCl crystals from crystal-nucleation data," Phys. Rev. Lett. **100**, 036103 (2008).